

Enhancement of Energy Transfer Efficiency with Structural Control of Multichromophore Light-Harvesting Assembly

Inhwan Oh, Hosoo Lee, Tae Wu Kim, Chang Woo Kim, Sunhong Jun, Changwon Kim, Eun Hyuk Choi, Young Min Rhee, Jeongho Kim,* Woo-Dong Jang,* and Hyotcherl Ihee*

Multichromophore systems (MCSs) are envisioned as building blocks of molecular optoelectronic devices. While it is important to understand the characteristics of energy transfer in MCSs, the effect of multiple donors on energy transfer has not been understood completely, mainly due to the lack of a platform to investigate such an effect systematically. Here, a systematic study on how the number of donors (n_D) and interchromophore distances affect the efficiency of energy transfer (η_{FRET}) is presented. Specifically, η_{FRET} is calculated for a series of model MCSs using simulations, a series of multiporphyrin dendrimers with systematic variation of n_D and interdonor distances is synthesized, and η_{FRET} s of those dendrimers using transient absorption spectroscopy are measured. The simulations predict η_{FRET} in the multiporphyrin dendrimers well. In particular, it is found that η_{FRET} is enhanced by donor-to-donor energy transfer only when structural heterogeneity exists in an MCS, and the relationships between the η_{FRET} enhancement and the structural parameters of the MCS are revealed.

example energy transfer, occurring in multichromophore systems (MCSs). In general, a multichromophore light-harvesting system consists of multiple donors, which can absorb light in a wide spectral range, and multiple acceptors, which can receive the absorbed energy from the donors. For the optimum performance of such a system, it would be desirable to achieve efficient donor-to-acceptor (D–A) energy transfer. Energy transfer between a donor and an acceptor is often explained by the mechanism of Förster resonance energy transfer (FRET).^[12] According to the FRET theory, the efficiency of energy transfer is inversely proportional to the sixth power of D–A distance,^[13–16] and therefore a donor–acceptor pair needs to be located within a certain distance for facilitating the transfer. While it would be ideal to achieve coherent energy transfer, it is difficult to precisely

1. Introduction

Light-harvesting systems consisting of multiple chromophores^[1] have recently attracted much interest as building blocks of molecular optoelectronic devices, for example, artificial light-harvesting assemblies,^[2–7] semiconductor and organic electronic materials,^[8] and photovoltaic solar cells.^[9–11] For the development and optimization of such devices, it is crucial to understand the physics and chemistry of dynamic processes, for

locate the donors and acceptors at positions required for coherent energy transfer to occur. In reality, incoherent energy transfer in the weak coupling regime is operational for most of MCSs.

For MCSs, however, there have been reports that the experimentally measured efficiency of excitation energy transfer (η_{FRET}), which is defined as the probability of the acceptor to receive the energy absorbed by the donor, is much lower than the theoretically predicted efficiency.^[17–22] It has been known that such a discrepancy in the experimental and theoretical η_{FRET}


I. Oh, Dr. T. W. Kim, Dr. C. W. Kim, C. Kim, E. H. Choi, Prof. Y. M. Rhee, Prof. H. Ihee
Department of Chemistry
Korea Advanced Institute of Science and Technology (KAIST)
Daejeon 34141, Republic of Korea
E-mail: hyotcherl.ihee@kaist.ac.kr

I. Oh, Dr. T. W. Kim, Dr. S. Jun, C. Kim, E. H. Choi, Prof. H. Ihee
Center for Nanomaterials and Chemical Reactions
Institute for Basic Science (IBS)
Daejeon 34141 Republic of Korea

I. Oh, Dr. T. W. Kim, C. Kim, E. H. Choi, Prof. H. Ihee
KI for the BioCentury
Korea Advanced Institute of Science and Technology (KAIST)
Daejeon 34141 Republic of Korea

H. Lee, Prof. W.-D. Jang
Department of Chemistry
College of Science
Yonsei University
Seoul 120-749 Republic of Korea
E-mail: wdjang@yonsei.ac.kr

Prof. J. Kim
Department of Chemistry
Inha University
Incheon 22212 Republic of Korea
E-mail: jkim5@inha.ac.kr

 The ORCID identification number(s) for the author(s) of this article can be found under <https://doi.org/10.1002/advs.202001623>

© 2020 The Authors. Published by Wiley-VCH GmbH. This is an open access article under the terms of the Creative Commons Attribution License, which permits use, distribution and reproduction in any medium, provided the original work is properly cited.

DOI: 10.1002/advs.202001623

is mainly caused by structural heterogeneity of the molecular systems,^[22–27] which becomes larger in complex MCSs. As an effort to compensate for the drop of η_{FRET} due to structural heterogeneity, many researchers have attempted to utilize donor-to-donor (D–D) energy transfer as a means of seeking the optimum path for efficient energy transfer toward acceptors.^[7,28] However, the influence of D–D energy transfer on η_{FRET} in MCSs has been controversial. For example, Olejko and Bald^[29] studied the effect of the number of donors (n_{D}) on η_{FRET} using the DNA origami structure as a scaffold for donors and acceptors. By varying n_{D} from one to four, they found that η_{FRET} barely changes with n_{D} although the amount of harvested energy increases with n_{D} . Buckhout-White et al.^[28] also investigated how n_{D} affects η_{FRET} by using the DNA structures of various shapes as a scaffold for donors and acceptor and observed only little improvement of η_{FRET} with the increase of n_{D} . In contrast, Trofymchuk et al.^[17] and Gartzia-Rivero et al.^[30] showed that, in polymeric nanoantennas composed of thousands of donors and a few acceptors, η_{FRET} increases with the increase of the weight ratio of donors to the mass of the polymer. Besides, there have been debates on whether the rate of D–D energy transfer influences η_{FRET} . Vijayakumar et al.^[31] showed that, for self-assemblies having different sizes of end functional groups, η_{FRET} increases with the increase of the rate of D–D energy transfer. In contrast, Melinger et al.^[21] reported that, for simple DNA dual-rail structures containing only one or two donors, η_{FRET} is enhanced with the aid of D–D energy transfer but only when the rate of D–D energy transfer is faster than the rate of D–A energy transfer. Also, they showed that, as long as the D–D energy transfer is fast enough, η_{FRET} does not change much with the change of the rate of D–D energy transfer. Since these discrepancies were observed in studies on different MCSs, a more systematic study is called for to establish a general principle that can be used to describe the energy transfer among multiple donors and acceptors.

In this work, to better understand how the presence of multiple donors influences η_{FRET} in MCSs, we comprehensively investigated energy transfer in a series of model MCSs by combining simulations, chemical synthesis, and time-resolved spectroscopy. We note that we employed the MCSs with the donors arranged in spherical symmetry, in contrast to the hybrid MCSs with donors arranged linearly as investigated in a previous study.^[32] In the linearly arranged donors, the D–A distance varies depending on the position of each donor. Since the D–A distance is the most critical factor that determines the FRET efficiency, we chose to investigate the spherically symmetric MCSs where the D–A distances are identical for all donors so that we can focus on the effect of homo-FRET on FRET efficiency. As the first step of such efforts, to account for the effect of d_{DA} , d_{DD} , and the orientation factor (κ^2) on η_{FRET} , we theoretically calculated η_{FRET} with simulations for a series of model MCSs consisting of multiple donors and a single acceptor while independently changing n_{D} and interchromophore distances, which include the D–A distance (d_{DA}) and the D–D distance (d_{DD}). Each simulation consists of Monte Carlo processes to calculate parameters needed to set up multiple differential equations, the solution of the differential equations to determine the time-dependent excited-state populations of donor and acceptor, and the calculation of the FRET efficiency. By running a sufficient number of simulations, we obtained η_{FRET} for various situations. Then, to experimentally check the validity of

the calculation results of model systems, we designed and synthesized various multiporphyrin dendrimers whose d_{DD} and n_{D} were independently adjusted, and measured the dynamics and efficiencies of energy transfer in the multiporphyrin dendrimers using femtosecond transient absorption (TA) spectroscopy. From our comprehensive study, we found that η_{FRET} is enhanced with the aid of D–D energy transfer and such enhancement is intricately related to the structural heterogeneity of MCSs, specifically the distributions of d_{DA} , d_{DD} , and κ^2 . The simulations presented in our study not only explain the seemingly contradicting results of previous studies but also predict η_{FRET} of various MCSs.

To simplify the calculation of η_{FRET} for an easy application to general MCSs of complicated structures, we employed the ideal dipole approximation (IDA),^[33,34] where the electronic coupling is described as the Coulombic interaction between transition dipole moments of donor and acceptor,^[35] instead of the exact calculation without any approximation. While IDA has limitations compared with the exact calculation,^[36] for the porphyrin dendrimers investigated in our work, it turned out that the η_{FRET} values calculated with IDA exhibit only $\approx 3.5\%$ deviation from the experimental η_{FRET} values.

2. Results

2.1. Calculation of η_{FRET} for Model Multichromophore Systems

To examine the effect of d_{DD} , d_{DA} , and n_{D} on η_{FRET} in MCSs, we calculated η_{FRET} for seven model systems that contain a single acceptor at the center and have multiple donors with various d_{DD} , d_{DA} , and n_{D} values, as shown in **Figure 1**. In the simulations, it was assumed that only a single donor per MCS was excited and the excitation probabilities of all donors were set to be equal. To effectively compare the energy transfer behavior in these MCSs of different chemical structures and various complexities, we define the normalized interchromophore distances, Δ_{DA} and Δ_{DD} , which are obtained by dividing d_{DA} and d_{DD} by the Förster radius for the D–A or D–D pair, respectively. To distinguish the donor-to-donor and donor-to-acceptor energy transfer, we denoted the D-to-A and the D-to-D energy transfer as “FRET” and “homo-FRET,” respectively.

While MCSs tend to have inherent structural heterogeneity, the distributions of structural parameters of those systems were not considered in previous studies.^[7,28–32,37] Structural heterogeneity can originate from both (i) the rapid structural fluctuation of orientation factor and interchromophore distance around each of their average values and (ii) the static distribution of structural parameters such as D–A distance and orientation factor of all donors. To consider the structural heterogeneity of MCSs, we performed the simulations for calculating η_{FRET} in the model MCSs while considering two cases for each of Δ_{DA} (and Δ_{DD}) and κ^2 , which are two major parameters that govern η_{FRET} , resulting in four cases in total. Specifically, for Δ_{DA} (and Δ_{DD}), we considered either a single value or a distribution of values. A single value means that all D–A (or D–D) pairs have the same Δ_{DA} (or Δ_{DD}) value, and a distribution means that those pairs can have different distance values from each other following a Gaussian distribution. For κ^2 , which is defined in the Experimental Section, we checked two representative cases: the dynamic and

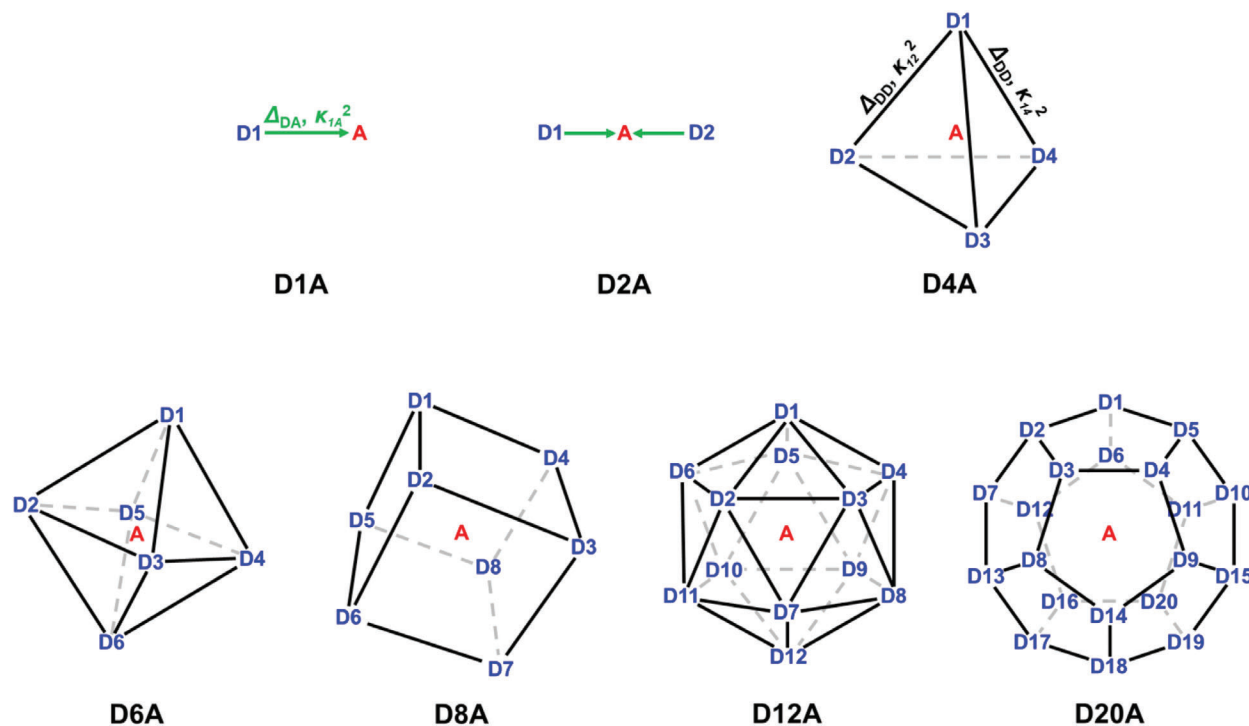


Figure 1. Seven model multichromophore systems used in simulations. In these model systems, the acceptor (A, red) is located at the center of multigonal structure formed by multiple donors (D, blue). The efficiency of energy transfer among chromophores is determined by the normalized interchromophore distances (Δ_{DA} and Δ_{DD}) and the orientation factor (κ^2). Detailed information on the seven model systems is described in the Experimental Section.

static isotropic limit. The dynamic isotropic limit refers to a condition where the transition dipoles rotate much faster than the time scale of energy transfer and, at this limit, κ^2 has a rotationally averaged value of $\frac{2}{3}$.^[23] In contrast, the static isotropic limit describes the condition where the transition dipoles rotate much slower than the time scale of energy transfer^[23] and thus κ^2 has a distribution of values. To summarize, as can be seen in Figure S14a,d in the Supporting Information, the following four cases were considered: i) a single value of Δ_{DA} (and Δ_{DD}) and the dynamic isotropic limit, ii) a single value of Δ_{DA} (and Δ_{DD}) and the static isotropic limit, iii) a finite distribution of Δ_{DA} (and Δ_{DD}) and the dynamic isotropic limit, and iv) a finite distribution of Δ_{DA} (and Δ_{DD}) and the static isotropic limit. Details of the simulations and the model systems are described in the Experimental Section.

The results of simulations are illustrated in **Figure 2**; and Figure S14 (Supporting Information). Initially, the simulations were performed under the simplest condition, case (i). In particular, we calculated η_{FRET} while varying Δ_{DA} or Δ_{DD} . As shown in Figure 2c, η_{FRET} increases with the decrease of Δ_{DA} in the D20A model, which is in good agreement with the one predicted by the Förster's equation for a single D–A pair. Here we define the degree of η_{FRET} enhancement induced by homo-FRET as $\Delta\eta_{FRET}$ by taking the difference between η_{FRET} values in D_nA model and D1A model. In case (i), as shown in Figure 2e,f, η_{FRET} is not enhanced at all, that is, $\Delta\eta_{FRET} = 0$, with the variation of Δ_{DA} , Δ_{DD} , or n_D . Next, the simulations were performed for the other three cases, where Δ_{DA} (and Δ_{DD}) and/or κ^2 have a distribution of values. As shown in Figure 2d; and Figure S14f–h, η_{FRET} tends to

increase with the decrease of Δ_{DA} , in agreement with case (i). However, in contrast to case (i), η_{FRET} is enhanced with the variation of Δ_{DA} or Δ_{DD} , that is, $\Delta\eta_{FRET} > 0$, in case (ii)–(iv). Specifically, $\Delta\eta_{FRET}$ becomes maximal at intermediate values of Δ_{DA} , as shown in Figure 2e; and Figure S14j–l. In addition, $\Delta\eta_{FRET}$ increases with the decrease of Δ_{DD} , but such increase is saturated below a certain threshold Δ_{DD} value, as shown in Figure 2f; and Figure S14n,p. Especially, it should be noted that $\Delta\eta_{FRET}$ is positive even when Δ_{DD} is larger than Δ_{DA} . In addition, $\Delta\eta_{FRET}$ increases with the increase of n_D , even in the Δ_{DD} region where the increase of $\Delta\eta_{FRET}$ is saturated. However, as shown in Figure 2f, $\Delta\eta_{FRET}$ does not simply increase with n_D when Δ_{DD} is larger than a certain limit. For example, $\Delta\eta_{FRET}$ of D20A is smaller than that of D12A at $\Delta_{DD} > 0.7$, indicating that the effect of n_D on η_{FRET} is saturated above a certain n_D value. These results of our simulations demonstrate that the presence of distributions for Δ_{DA} , Δ_{DD} , and κ^2 values as in case (ii)–(iv) induces the enhancement of η_{FRET} (that is, $\Delta\eta_{FRET} > 0$), indicating that the $\Delta\eta_{FRET}$ is closely related to the structural heterogeneity of MCSs. The results of the simulations are further discussed in detail in the Discussion section and the Supporting Information.

2.2. Design of Multiporphyrin Dendrimers

To experimentally test the validity of the results of simulations, we designed and synthesized the MCSs with various n_D and d_{DD} values. Since it is difficult to experimentally prepare the ideal

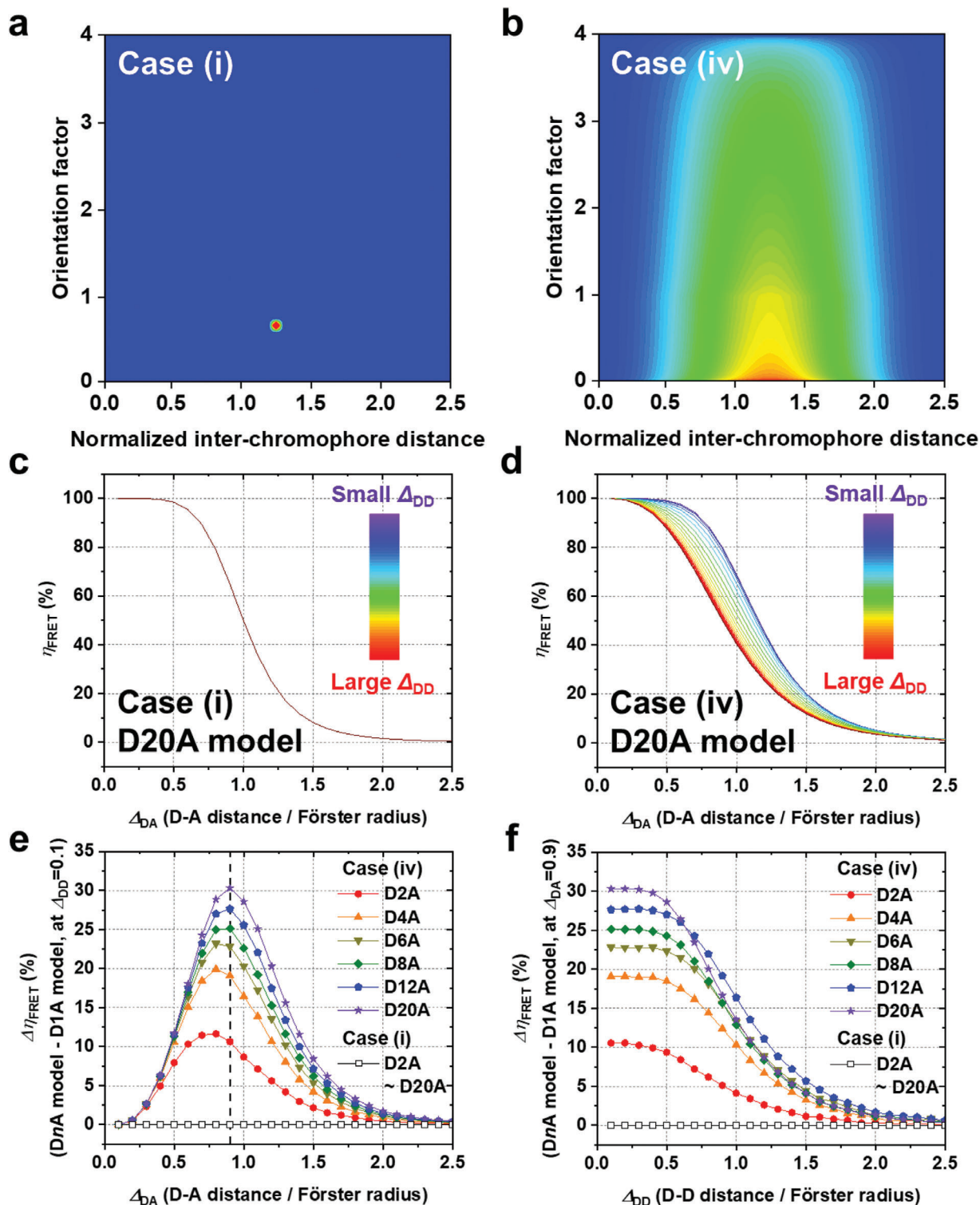


Figure 2. Simulation for calculating η_{FRET} in model MCSs. a,b) Schematic of distributions of the interchromophore distances and the orientation factor in cases (i) and (iv) used in our simulations. The distributions are shown in the form of heat maps where blue and red indicate the lowest and highest values. c,d) The FRET efficiency (η_{FRET}) of D20A as a function of Δ_{DA} for various Δ_{DD} values. η_{FRET} was calculated with given values of Δ_{DA} , Δ_{DD} , and κ^2 . η_{FRET} curves for various Δ_{DD} values are plotted following a rainbow color scheme, from red (the largest Δ_{DD}) to purple (the smallest Δ_{DD}). e) $\Delta\eta_{\text{FRET}}$ of DnA relative to D1A, that is $\eta_{\text{FRET}}(\text{DnA}) - \eta_{\text{FRET}}(\text{D1A})$, as a function of Δ_{DA} with the shortest Δ_{DD} ($= 0.1$) for D2A (red), D4A (orange), D6A (dark yellow), D8A (green), D12A (blue), and D20A (violet). f) $\Delta\eta_{\text{FRET}}$ as a function of Δ_{DD} with $\Delta_{\text{DA}} = 0.9$, where $\Delta\eta_{\text{FRET}}$ is maximized for D20A. In both (e) and (f), results of case (iv) are indicated by filled symbols and those of case (i) are indicated by open symbols. All $\Delta\eta_{\text{FRET}}$ curves for case (i) have zero values for all Δ_{DA} and Δ_{DD} regardless of η_{D} . The simulation results of case (ii) and case (iii) are shown in Figure S14 (Supporting Information).

forms of MCSs as the ones used for the simulations, we instead prepared multiporphyrin dendrimers as the model compounds. The multiporphyrin dendrimers should be an excellent model system because both n_D and d_{DD} can be adjusted independently by controlling the type, number, and position of linkers while keeping d_{DA} and the spectral overlap integral for D–A pairs unchanged for each donor.^[6,38] In this context, we synthesized a total of six multiporphyrin dendrimers with various combinations of n_D and d_{DD} values, as illustrated in **Figure 3**. For example, SD4A, MD4A, and LD4A have the same n_D value but different d_{DD} values, and MD2A, MD4A, and MD8A have the same d_{DD} value but different n_D values. The absorption and emission spectra of dendrimers and their constituent donor and acceptor units are shown in **Figure 3c,d**. The weak electronic coupling between ground-state porphyrins in dendrimers was confirmed by the absence of the spectral broadening or shift in their spectra. The Förster radius for the D–A pair was calculated to be 2.43 nm from the static spectroscopic data, as described in the Supporting Information.

To estimate the equilibrium structures of the dendrimers, molecular dynamics (MD) simulations were performed for the multiporphyrin dendrimers. The results of MD simulations are shown in **Figure 4**, and details of MD simulations are described in the Supporting Information. According to the MD simulation, the distributions of d_{DA} are similar for all donors in a dendrimer, as shown in **Figure 4a**, and the averaged d_{DA} distributions for all donors in a dendrimer are similar for all of the dendrimers, as shown in **Figure 4b**. This result suggests that the mean d_{DA} of all dendrimers does not change regardless of the variation of d_{DD} and n_D . Unlike d_{DA} , however, the averages of d_{DD} distributions are different for each pair of donors, depending on their geometry in a dendrimer, as shown in **Figure 4c**. Therefore, in these dendrimers, we can clearly examine the effect of d_{DD} and n_D on η_{FRET} , independent of d_{DA} . The structural information on the porphyrin dendrimers obtained from the MD simulations was used as input for calculating the theoretical η_{FRET} for the dendrimers using the simulations described above.

2.3. FRET Efficiencies of Multiporphyrin Dendrimers

To measure the dynamics of energy transfer in the multiporphyrin dendrimers, femtosecond TA spectroscopy^[39] was employed, as described in the Experimental Section. The results of TA measurement for multiporphyrin dendrimers and monomeric zinc porphyrin are shown in **Figure 5**; and **Figure S10** (Supporting Information). In **Figure 5**, it can be seen that the TA spectra of the monomeric zinc porphyrin exhibit the decay of the 1.3 ns time constant. Considering the characteristic spectral evolution shown in decay associated spectra and that the singlet excited state of zinc porphyrin species mainly decays via intersystem crossing to a triplet state rather than fluorescence emission, we can assign the TA decay of monomeric zinc porphyrin to intersystem crossing.^[40–44] Unlike the spectral evolution of the monomeric zinc porphyrin, the TA spectra of dendrimers show distinct and fast spectral changes. The ground state bleach (GSB) of donor (543 nm) is reduced, while the GSB of acceptor (517 nm) is increased, and the SE of donor (637 nm) is shifted to longer

wavelengths. Based on these features, we attribute the spectral changes of dendrimers to the FRET from donors to the acceptor.

To characterize the dynamics of the time-dependent spectral changes in the TA spectra of various dendrimers, we globally fitted the TA spectra in the entire spectral range of our measurement. The resultant decay-associated spectra (DAS) of the monomeric zinc porphyrin and MD2A are shown in **Figure 5c,d**, respectively, and the temporal decays of those DAS are shown in **Figure 5e,f**.^[45] Since there exist multiple donor–acceptor pairs in each dendrimer and d_{DA} has a distribution of values rather than a single value, the dendrimers are expected to exhibit complex, parallel energy transfer dynamics, as manifested in **Figure 5f**.^[46] To reflect such complicated dynamics, we fitted the decay of TA spectra using a stretched exponential function, which is suitable for describing a relaxation process that takes place in a parallel manner with varying time scales

$$I_{TA}(t) = A \times e^{-(t/\tau_{DA})^\beta} + I_{\text{long}}$$

where τ_{DA} is the time constant of FRET process and β is related to the degree to which the exponential function is stretched. The fit parameters are presented in **Table 1**, and η_{FRET} was calculated using Equation (4).^[47,48] It can be seen that, for various dendrimers, η_{FRET} differs by up to 11%. Especially, η_{FRET} of MD8A is higher than those of MD4A and MD2A although these three dendrimers have identical mean values of d_{DD} and d_{DA} . For the three dendrimers having four donors (SD4A, MD4A, and LD4A), it can also be seen that η_{FRET} of a dendrimer with shorter d_{DD} is larger than that of a dendrimer with longer d_{DD} . These results show that η_{FRET} of a dendrimer is enhanced by the increase of n_D or the decrease of d_{DD} .

To verify whether the simulations accurately describe the FRET dynamics in MCSs, we predicted the theoretical η_{FRET} of the multiporphyrin dendrimers with the simulations using the structural information obtained from the MD simulations. Details of the calculation of theoretical η_{FRET} are described in the Supporting Information. For each dendrimer, the theoretical η_{FRET} is compared with the experimentally determined η_{FRET} . As shown in **Table 1**, the theoretical η_{FRET} s agree well with the experimental η_{FRET} s, but overall they are underestimated by $\approx 3.5\%$ compared with the experimental η_{FRET} s. These discrepancies might be attributed to the limitation of IDA applied to the Förster's equation and the slight inaccuracy of the d_{DA} value obtained from MD simulations. Therefore, we varied d_{DA} to match the theoretical η_{FRET} with the experimental value and calculated the modified theoretical η_{FRET} s. The modified theoretical and the experimental η_{FRET} s were in agreement with each other when the d_{DA} value of 1.65 nm were used, instead of 1.69 nm. The excellent agreement of the modified theoretical and the experimental η_{FRET} s implies that our simulations well describes the FRET behavior in MCSs.

3. Discussion

The excitation energy of donors can be transferred to the acceptor either directly or through multiple steps involving homo-FRET among donors. If the energy transfer via these detour paths involving homo-FRET is more efficient than the direct transfer to

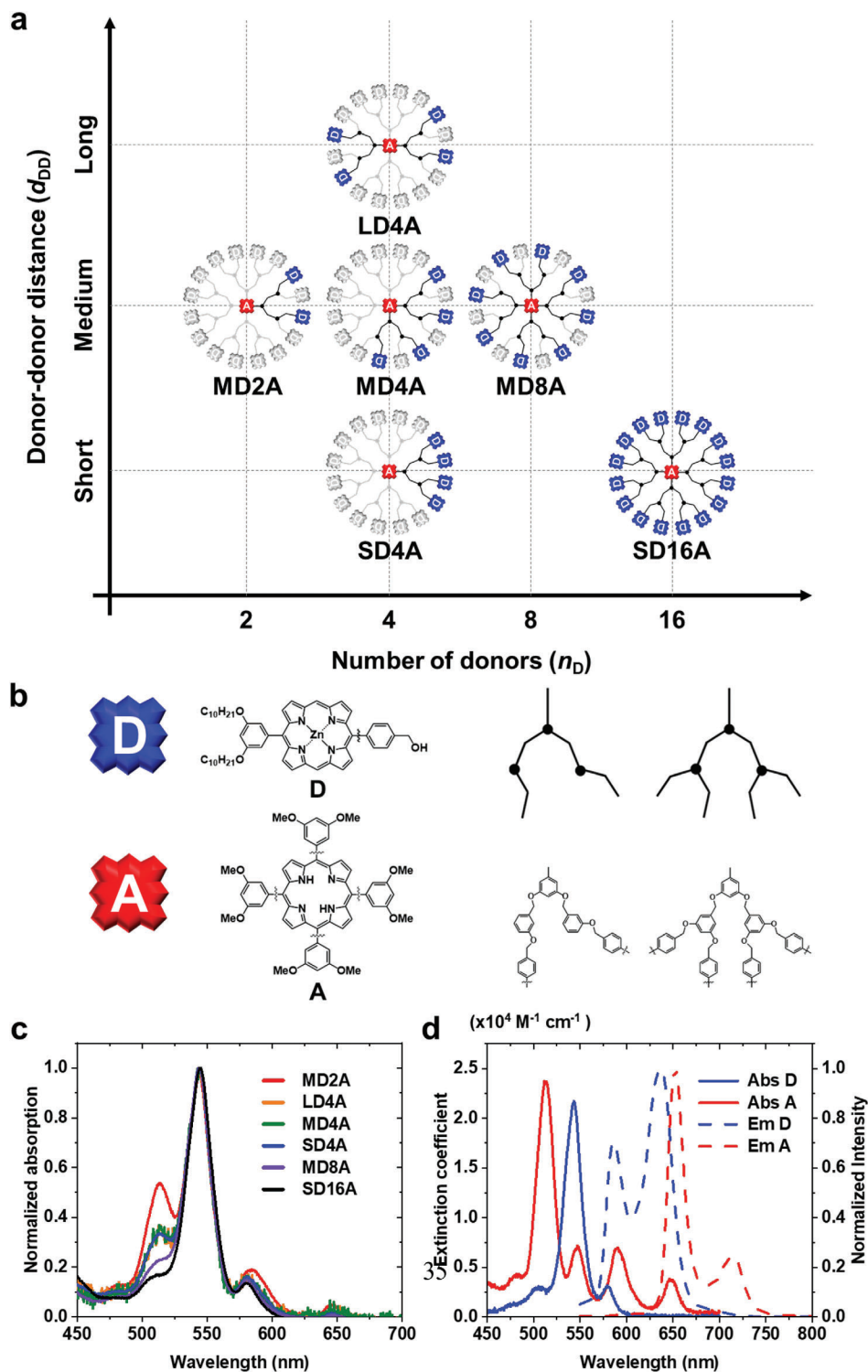


Figure 3. Structures of multiporphyrin dendrimers and their structural units. a) Molecular structures of multiporphyrin dendrimers used in this study represented as a function of n_D and d_{DD} . The actual structures of the dendrimers are 3D rather than planar, but they are depicted as the planar configurations for the sake of clear presentation. In all of the six dendrimers, each zinc porphyrin donor (D, blue) is connected to a free-base porphyrin acceptor (A, red) by the linker of the same length. For easier comparison among the dendrimers, the structures of all the dendrimers are drawn on the same frame as SD16A, and the spots without any chromophore are indicated in gray. A dendrimer containing short D–D pairs is labeled as S, a dendrimer containing long D–D pairs without any short D–D pair is labeled as L, and all other dendrimers without any short or long D–D pairs are labeled as M. b) Molecular structures of zinc porphyrin donor (D) unit, free-base porphyrin acceptor (A) unit, and linkers connecting the D and A units in the multiporphyrin dendrimers. c) Normalized absorption spectra of multiporphyrin dendrimers. d) Absorption and emission spectra of monomeric donor and acceptor.

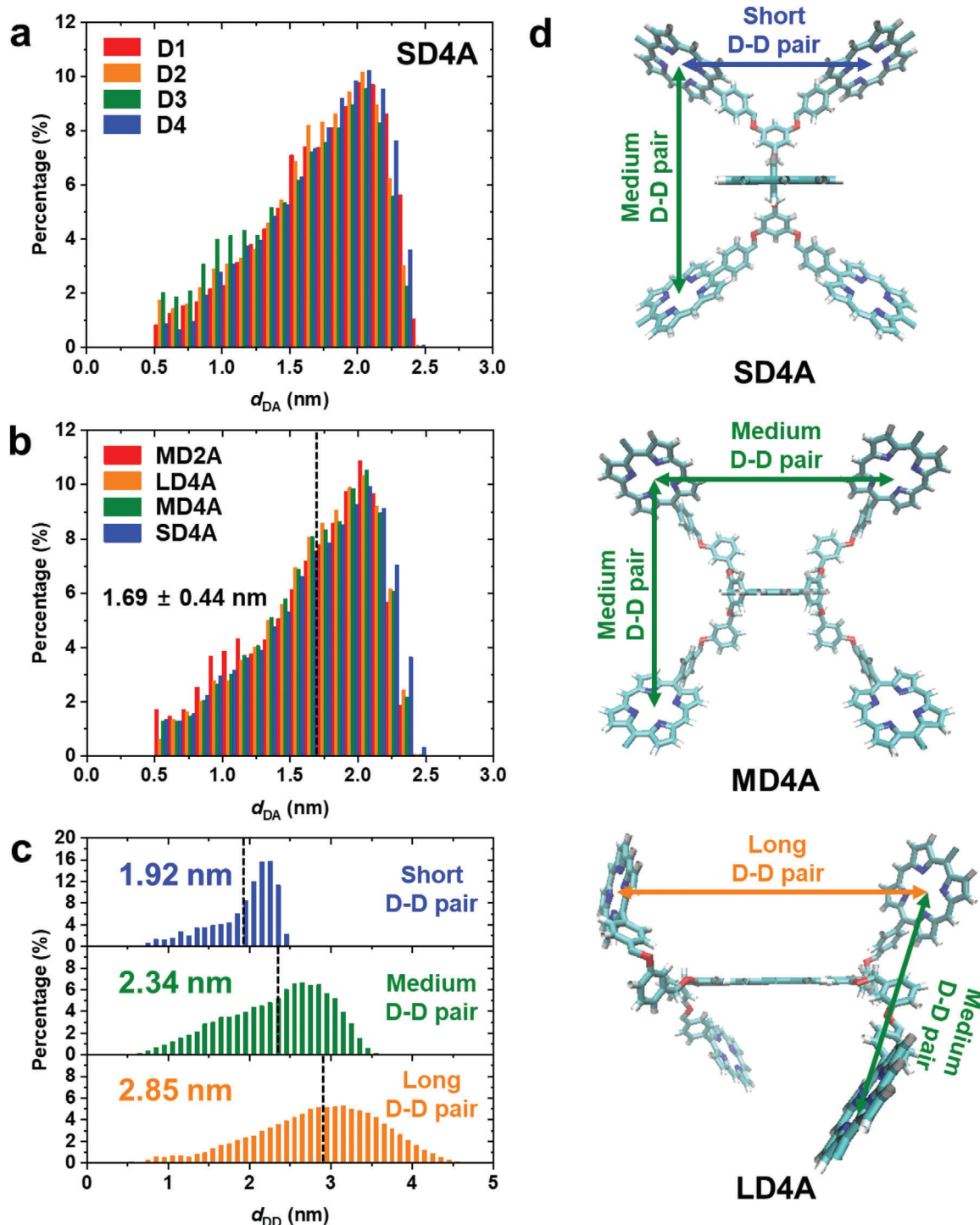


Figure 4. Distributions of d_{DA} and d_{DD} of multiporphyrin dendrimers obtained from MD simulations. a) Distributions of d_{DA} for each of the four donors in SD4A. b) Averaged distributions of d_{DA} for MD2A, LD4A, MD4A, and SD4A. The mean value of all the averaged d_{DA} distributions for the six dendrimers is 1.69 ± 0.44 nm. c) Averaged distributions of d_{DD} for short D–D pairs (blue), medium D–D pairs (green), and long D–D pairs (orange) in all six dendrimers. The classification into short, medium, and long D–D pairs are defined in the caption of Figure 3a. The mean value of each averaged d_{DD} distribution is indicated by a dashed line. Examples of short, medium, and long D–D pairs are illustrated in (d). d) Average structures of multiporphyrin dendrimers with four donors. The positions of each D–D pair are indicated. For MD4A, the distance between donors attached to different linkers from the acceptor (2.44 nm) is slightly longer than the distance between donors connected with the same linker from the acceptor (2.34 nm) although both pairs of donors are classified into medium D–D pairs.

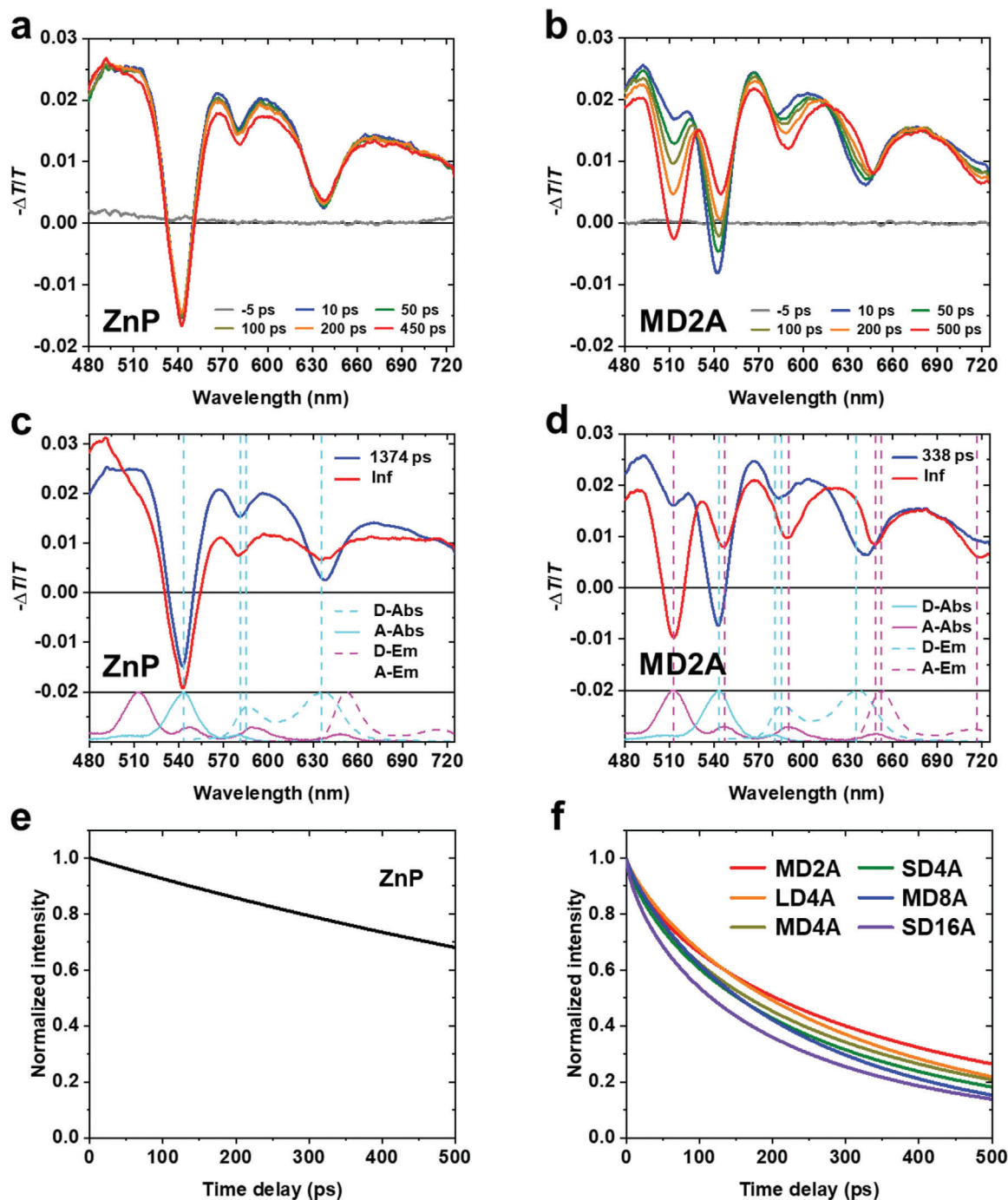


Figure 5. Transient absorption (TA) spectra and decay-associated spectra (DAS) of monomeric zinc porphyrin and MD2A dendrimer. a,b) TA spectra of the monomeric zinc porphyrin (a) and MD2A (b) at various time delays. c,d) DAS of the monomeric zinc porphyrin (c) and MD2A (d) obtained from the global target analysis of TA spectra. The steady-state absorption spectra (solid line) and emission spectra (dashed line) of the donor (cyan) and the acceptor (magenta) are shown together at the bottom. The vertical dashed lines indicate the peak positions of steady-state absorption and emission spectra. Temporal decay of the DAS of e) monomeric zinc porphyrin and f) multiporphyrin dendrimers.

the acceptor, η_{FRET} will be enhanced compared with when homo-FRET does not occur. From the simulations of energy transfer for the seven model systems, we comprehensively examined how various structural parameters (n_{D} , Δ_{DD} , Δ_{DA} , and κ^2) of an MCS affects η_{FRET} . In particular, we emphasize how structural hetero-

geneity in an MCS affects η_{FRET} by comparing case (i) and the other three cases.

According to previous studies, structural heterogeneity tends to deteriorate η_{FRET} .^[22–28] However, as can be seen in Figure 2; and Figure S14 (Supporting Information), η_{FRET} can be enhanced

Table 1. Summary of the time constants and β values observed in TA spectra of multiporphyrin dendrimers and calculated FRET efficiency (η_{FRET}).

	$\tau_{\text{DA}}^{\text{a)}$ [ps]	$\beta^{\text{b)}$	Experimental $\eta_{\text{FRET}}^{\text{b)}$ [%]	Theoretical $\eta_{\text{FRET}}^{\text{c)}$ [%]	Modified theoretical $\eta_{\text{FRET}}^{\text{d)}$ [%]
MD2A	338 ± 29	0.73 ± 0.03	74.0 ± 2.2	72.1	74.1
LD4A	302 ± 4	0.83 ± 0.02	76.8 ± 0.3	74.7	76.5
MD4A	273 ± 4	0.75 ± 0.02	79.0 ± 0.3	77.0	78.6
SD4A	248 ± 18	0.76 ± 0.04	80.9 ± 1.4	78.2	79.8
MD8A	238 ± 17	0.85 ± 0.05	81.7 ± 1.3	78.8	80.4
SD16A	194 ± 15	0.72 ± 0.05	85.1 ± 1.1	83.9–85.8	85.2–87.1

^{a)}All FRET time constants (τ_{DA}) and β values were determined from the global fits of the first and second right singular vectors of TA spectra ^{b)}Experimental η_{FRET} s were calculated from the time constants obtained from TA measurements by using Equation (S4) (Supporting Information). We note that the decay time constant of the TA spectra of monomeric zinc porphyrins is 1.3 ns ^{c)}Theoretical η_{FRET} s were calculated with the simulations using the structural information of dendrimers obtained from MD simulations. We note that the mean value (1.69 nm) of the d_{DA} distribution in Figure 4b was used ^{d)}Modified theoretical η_{FRET} s were calculated with the simulations using the d_{DA} value of 1.65 nm, instead of 1.69 nm. The d_{DA} value of 1.65 nm was obtained, while we vary d_{DA} to match the theoretical η_{FRET} with the experimental value. Based on the good agreement of the modified theoretical and experimental η_{FRET} s, we can infer that the value of 1.65 nm is the effective d_{DA} in the multiporphyrin dendrimers.

with the aid of structural heterogeneity caused by the presence of multiple donors and homo-FRET among donors. As shown in Figure 2f; and Figure S14n,o (Supporting Information), η_{FRET} is enhanced with the decrease of Δ_{DD} in case (ii), (iii), and (iv), implying that the increase of the homo-FRET rate (due to the decrease of Δ_{DD}) activates more detour FRET paths of high efficiencies. As mentioned in the simulation results, the increase of $\Delta\eta_{\text{FRET}}$ with the decrease of Δ_{DD} is saturated below a certain threshold Δ_{DD} value, of which the reason is discussed in Note S8 (Supporting Information). Considering that the enhancement of η_{FRET} is not observed in case (i), we can infer that structural heterogeneity in the MCS plays an important role in the enhancement of η_{FRET} induced by homo-FRET. In case (i), η_{FRET} does not change at all with the variation of n_{D} or Δ_{DD} , suggesting that homo-FRET does not affect the FRET efficiency without any structural heterogeneity. In contrast, in cases (ii), (iii), and (iv) with heterogeneity of Δ_{DA} (and Δ_{DD}) and/or κ^2 , $\Delta\eta_{\text{FRET}}$ is positive and changes sensitively with the variation of n_{D} and Δ_{DD} , indicating the strong influence of structural heterogeneity on the homo-FRET-induced enhancement of η_{FRET} . Thus, according to our simulations, only when there exists structural heterogeneity in an MCS, homo-FRET enhances η_{FRET} , thus compensating for the loss of η_{FRET} induced by the structural heterogeneity to some extent.

While we demonstrated that structural heterogeneity is essential for the homo-FRET-induced enhancement of η_{FRET} , it would be desirable to describe their relationship quantitatively. If we define the FRET efficiency, Φ_{FRET} , of an individual donor, the structural heterogeneity in an MCS can be manifested as a distribution of Φ_{FRET} for multiple donors. In other words, when there exists structural heterogeneity, the distribution of Φ_{FRET} would have a finite width. While η_{FRET} is enhanced in cases (ii), (iii), and (iv), where Φ_{FRET} has a distribution of values, the Δ_{DA} dependences of $\Delta\eta_{\text{FRET}}$ for those three cases are different from each other, as shown in Figure 2e; and Figure S14j,k (Supporting Information), because the distribution of Φ_{FRET} arises from different origins in those three cases. For case (ii), the distribution of Φ_{FRET} is governed by only the distribution of κ^2 . For case (iii), the distribution of Φ_{FRET} is governed by only the distribution of Δ_{DA} . For case (iv), the distribution of Φ_{FRET} is governed by the distributions of both κ^2 and Δ_{DA} . At $\Delta_{\text{DA}} > 1.5$ in case (ii) and at $\Delta_{\text{DA}} < 0.4$ in case (iii), $\Delta\eta_{\text{FRET}}$ induced by homo-FRET is negligibly small. Such limited enhancement of η_{FRET} in those Δ_{DA} regions indicates that the distribution of Φ_{FRET} is too narrow to enhance η_{FRET} . In fact, it can be seen in Figure S17 (Supporting Information) that $\Delta\eta_{\text{FRET}}$ is governed by the width of Φ_{FRET} distribution for cases (ii) and (iii). In contrast, in case (iv), η_{FRET} is enhanced in the entire Δ_{DA} region because the variation of κ^2 and the variation of Δ_{DA} induces the enhancement of η_{FRET} at small and large Δ_{DA} values, respectively, thus complementing each other. In other words, in case (iv), the distributions of both κ^2 and Δ_{DA} contribute to the enhancement of η_{FRET} , as confirmed by Figure S18 (Supporting Information). Further discussions on the dependence of η_{FRET} on Δ_{DA} are described in Notes S7 and S8 (Supporting Information).

As shown in Figure 2e; and Figure S14j,k (Supporting Information), η_{FRET} is enhanced overall by the increase of n_{D} , in the order of D2A, D4A, D6A, D8A, D12A, and D20A. Such dependence of η_{FRET} on n_{D} can be attributed the increase of donors that are available for homo-FRET. However, it is noteworthy that the

$\Delta\eta_{\text{FRET}}$ is not exactly proportional to n_{D} when Δ_{DD} is larger than ≈ 0.7 , as shown in Figure 2f; and Figure S14n,o (Supporting Information). For example, at $\Delta_{\text{DD}} = 1.3$, the $\Delta\eta_{\text{FRET}}$ increases in the order of D2A, D4A, D8A, D20A, D6A, and D12A, as shown in Figure S21 (Supporting Information). To find the origin of the deviation from the dependence on n_{D} , we checked how the average homo-FRET efficiency depends on Δ_{DD} . At $\Delta_{\text{DD}} = 0.1$, both the average homo-FRET efficiencies to the nearest and the second nearest donors are close to 100%. By contrast, at $\Delta_{\text{DD}} = 1.3$, the average efficiency of homo-FRET to the nearest donors is 20%, while that to the second-nearest donors is only 5% at best. Such a large difference in the homo-FRET efficiencies between the nearest and the second-nearest donors means that only homo-FRET to the nearest donors is effective. Base on this observation, for all model systems, we checked the number of the nearest donors (n_{ND}), which is 2, 3, 3, 3, 4, and 5 for D2A, D4A, D8A, D20A, D6A, and D12A, respectively. Indeed, the order of the model systems in terms of n_{ND} exactly matches the observed order of model systems in terms of η_{FRET} , indicating that η_{FRET} is governed by n_{ND} rather than n_{D} , the total number of donors. To further verify the influence of n_{ND} on η_{FRET} , we also performed simulations for pseudomodel systems where all donors are equally spaced from each other, that is, n_{ND} equals n_{D} . As shown in Figure S22 (Supporting Information), the simulation results show that the $\Delta\eta_{\text{FRET}}$ is proportional to n_{D} for such model systems. Thus, the $\Delta\eta_{\text{FRET}}$ is governed n_{ND} rather than n_{D} . Ultimately, the 3D arrangement of chromophores and the extent of structural heterogeneity in an MCS would be important factors that determine the homo-FRET-induced enhancement of η_{FRET} because n_{ND} would be determined by these factors.

We can compare our simulation results with those of the previous studies, as discussed in Note S9 (Supporting Information). Notably, the simulations performed in a previous spectroscopic study on DNA-fluorophore MCSs showed that when d_{DD} is increased by 54% from 13 Å ($\Delta_{\text{DD}} = 0.25$) to 20 Å ($\Delta_{\text{DD}} = 0.38$), η_{FRET} changes only by 3% and suggested that η_{FRET} is not much affected by the rate of homo-FRET, as long as the homo-FRET rate is significantly faster than the hetero-FRET rate.^[21] These results are consistent with ours. Such insensitivity of η_{FRET} to Δ_{DD} should be attributed to the limited Δ_{DD} range (0.25–0.38) examined in that study. As can be seen in Figure 2f, our simulations show that $\Delta\eta_{\text{FRET}}$ is saturated in that Δ_{DD} range. On the other hand, based on their own simulation, they inferred that the enhancement of η_{FRET} induced by homo-FRET occurs only when homo-FRET is faster than FRET. By contrast, our simulations suggest that η_{FRET} can be enhanced even when Δ_{DD} is larger than Δ_{DA} (that is, homo-FRET is slower than FRET), as can be seen in Figure 2f ($\Delta\eta_{\text{FRET}} > 0$ at $\Delta_{\text{DD}} > \Delta_{\text{DA}}$). This result of our simulations implies that homo-FRET still effectively funnels the excitation energy toward the detour FRET paths of high efficiencies even when homo-FRET is slower than FRET. In agreement with this result of our simulation, our TA measurements show that η_{FRET} is enhanced in the dendrimers investigated in this work, all of which have smaller Δ_{DA} (0.7) than Δ_{DD} (1.0 for SD4A and SD16A, 1.2 for MD2A, MD4A, and MD8A and 1.5 For LD4A). In a similar study on MCSs based on DNA origami structure,^[29] η_{FRET} was determined from the measured fluorescence lifetime of the donor, while n_{D} being varied from one to four, and it was found that η_{FRET} was barely affected by the increase of n_{D} . This observation can be

easily rationalized by noting that these MCSs correspond to conditions where η_{FRET} is hardly affected by n_{D} . Similarly, in a study on MCSs consisting of various DNA networks,^[28] it was found that η_{FRET} does not show clear dependence on n_{D} . Here we can interpret that such insensitivity of η_{FRET} with respect to n_{D} can be attributed to the low formation efficiency of some of the MCSs used in that study. In fact, when only the MCSs of high formation efficiencies are considered, it can be clearly seen that η_{FRET} is enhanced with the increase of n_{D} . In addition, for the MCSs of high formation efficiencies, Δ_{DA} dependence of $\Delta\eta_{\text{FRET}}$ is also in good agreement with the results of our simulations. Thus, our simulations can account for the conflicts of the previous studies and serve as a tool that properly describes the η_{FRET} in MCSs.

We note that we used IDA for all of the simulations. One of the limitations of IDA is that it cannot account for the energy transfer between orthogonal chromophores, which should be treated by taking into account molecular vibrations and environmental fluctuations.^[49–53] The error caused by IDA generally increases with the decrease of the d_{DA} distance and the increase of the size of the chromophore.^[36] The porphyrin dendrimers investigated in our work have d_{DA} of 16.9 Å and the porphyrin unit has a size of ≈ 7 Å,^[54,55] giving the D–A separation of ≈ 2.4 in molecular size unit. According to the previous work,^[36] with this D–A separation value, the error is estimated to be $\approx 7.5\%$, which is comparable to the $\approx 3.5\%$ deviation between the η_{FRET} estimated using IDA and the experimentally measured value in our work. Since such an error due to IDA will apply to all porphyrin dendrimers systematically, it should not affect the relative η_{FRET} of the porphyrin dendrimers, which is of our interest in this work. In fact, the variation of the calculated η_{FRET} for different porphyrin dendrimers is in excellent agreement with the trend of the experimentally measured values for those dendrimers (see Table 1). While the correction using the exact approach instead of IDA will reduce the error, our approach using IDA requires only simple calculation and can be easily applied to MCSs of various chemical structures.

4. Conclusion

Based on the simulations on model MCSs for four different cases and the TA measurements on multiporphyrin dendrimers, we revealed the followings on the energy transfer efficiencies and the structural parameters of the MCSs: i) η_{FRET} is enhanced by homo-FRET only when there exists structural heterogeneity in the MCS; ii) the enhancement of η_{FRET} is directly related to the distribution of Φ_{FRET} , of which the width is governed by the distribution of κ^2 at small Δ_{DA} values and by the distribution of Δ_{DA} at large Δ_{DA} values; iii) η_{FRET} is enhanced by the increase of n_{D} , especially by the increase of n_{ND} . Based on these lessons learned from this study, we can explain why the conclusions from previous studies seemingly conflict with each other. The excellent agreement between the experimental and the calculated η_{FRET} s (see Table 1) demonstrated for the systematically designed MCSs investigated in our study would provide a principle for accurately predicting η_{FRET} in various MCSs. Our findings can help a better understanding of energy transfer in MCSs, including natural light-harvesting systems, and provide a design principle for novel optoelectronic devices.

5. Experimental Section

Calculation of η_{FRET} for Model Multichromophore Systems: For each model MCS, η_{FRET} was calculated at given Δ_{DA} and Δ_{DD} values by averaging Φ_{FRET} , the FRET efficiency of an individual donor, obtained from 100,000 simulations, which are large enough to sample the distributions of structural parameters. Each simulation consists of the Monte Carlo processes to calculate the parameters necessary for setting up multiple differential equations to determine the time-dependent excited-state populations of donor and acceptor, the solution of the differential equations which provide the excited-state populations of chromophores as a function of time at given Δ_{DA} and Δ_{DD} values, and the calculation of Φ_{FRET} , by dividing the final excited-state population of the acceptor by the initial excited-state population of the donor. For the calculation of Φ_{FRET} , it was assumed that the intrinsic decay rate of the excited-state population of the acceptor was negligibly small. Under this condition, the excited-state population of the acceptor was changed only by FRET from the donor. For each model MCS, such simulations were performed for all four cases discussed in the main text (cases (i)–(iv)). For cases (i) and (ii) where Δ_{DA} (and Δ_{DD}) has a single value, 25 Δ_{DA} values and 25 Δ_{DD} values were used between 0.1 and 2.5 with the increment of 0.1. For cases (iii) and (iv) where Δ_{DA} (and Δ_{DD}) has a finite distribution, a random number was generated for Δ_{DA} (and Δ_{DD}) following its Gaussian distribution. The mean value of the Gaussian distribution was increased from 0.1 to 2.5 with an increment of 0.1. The relative standard deviation of the Gaussian distribution was set to be 0.2.

In general, MCSs are composed of various types of chromophores. For simplicity, however, only a single type of energy-donor chromophore and a single type of energy-acceptor chromophore were considered for seven ideal model MCSs investigated in the study. In those model systems, an acceptor is surrounded by donors that are located as far apart from each other as possible. Each donor can have a distribution of Δ_{DA} for cases (iii) and (iv), but the mean Δ_{DA} s for all donors were set to be identical for all donors so that the effect of the variation of Δ_{DA} on η_{FRET} can be excluded. In addition, the mean Δ_{DD} s between the nearest donors were also set to be identical for all pairs of the nearest donors. For simulations on model MCSs with the number of n_{ND} set to be the same as n_{D} , the mean Δ_{DD} s among all pairs of donors were set to be equal. In the simulations, the excitation probabilities of all donors were set to be equal, but the simultaneous excitation of two or more donors was not considered. The direct excitation of the acceptor was not considered, either. The unidirectional D–A energy transfer as well as the D–D energy transfer were considered.

Energy transfer among multiple chromophores of two different types cannot be described only with a single Förster's equation but can be described with a combination of multiple Förster's equations. Therefore, differential equations that describe energy transfer for a model MCS consisting of n donors and a single acceptor can be expressed as follows

$$\begin{aligned} \frac{dD_a(t)}{dt} &= -\left(k_{\text{D}} + k_{\text{D}_a\text{A}} + k_{\text{D}_a\text{D}_b} + k_{\text{D}_a\text{D}_c} + \dots\right) D_a(t) + k_{\text{D}_b\text{D}_a} D_b(t) \\ &\quad + k_{\text{D}_c\text{D}_a} D_c(t) + \dots \\ \frac{dD_b(t)}{dt} &= -\left(k_{\text{D}} + k_{\text{D}_b\text{A}} + k_{\text{D}_b\text{D}_a} + k_{\text{D}_b\text{D}_c} + \dots\right) D_b(t) + k_{\text{D}_a\text{D}_b} D_a(t) \\ &\quad + k_{\text{D}_c\text{D}_b} D_c(t) + \dots \\ &\vdots \\ \frac{dA(t)}{dt} &= -k_{\text{A}} + k_{\text{D}_a\text{A}} D_a(t) + k_{\text{D}_b\text{A}} D_b(t) + \dots \\ &\quad (a, b, c, \dots = 1, 2, 3, \dots n, a \neq b \neq c \neq \dots) \end{aligned}$$

where $D_i(t)$ and $A(t)$ denote the excited-state populations of the i th donor and the acceptor, respectively; k_{DA} and k_{DD} denote the rate constants of

FRET and homo-FRET, respectively; k_{D} and k_{A} are the inverse of intrinsic lifetimes of the singlet excited states of the donor and the acceptor, respectively.

Prior to solving the multiple differential equations shown in Equation (2), the rate constants (e.g., k_{D} , k_{DA} , $k_{\text{D}_a\text{D}_b}$) included in the equations must be determined. Each rate constant is determined by k_{D} , κ^2 , and Δ_{DA} (and Δ_{DD}), as shown in the following equation

$$\begin{aligned} k_{\text{D}_a\text{A}} &= \frac{3}{2} \times k_{\text{D}} \times \kappa^2 \times \frac{1}{\Delta_{\text{DA}}^6}, \quad (a = 1, 2, 3, \dots n) \\ k_{\text{D}_a\text{D}_b} &= \frac{3}{2} \times k_{\text{D}} \times \kappa^2 \times \frac{1}{\Delta_{\text{DD}}^6}, \quad (a, b = 1, 2, 3, \dots n, a \neq b) \\ \Delta_{\text{DA}}^6 &= \left(\frac{d_{\text{DA}}}{R_0(\text{DA})}\right)^6, \quad \Delta_{\text{DD}}^6 = \left(\frac{d_{\text{DD}}}{R_0(\text{DD})}\right)^6 \\ \bar{R}_0(\text{DA})^6 &= \frac{3 \ln 10}{64\pi^5 N_{\text{A}}} \frac{Q_{\text{D}}}{n^4} J_{\text{DA}}, \quad \bar{R}_0(\text{DD})^6 = \frac{3 \ln 10}{64\pi^5 N_{\text{A}}} \frac{Q_{\text{D}}}{n^4} J_{\text{DD}} \end{aligned} \quad (3)$$

where κ^2 is the orientation factor, which is the relative orientation between the transition dipole moments of the donor and acceptor chromophores; d_{DA} and d_{DD} are the D–A and D–D distances, respectively; Δ_{DA} and Δ_{DD} are normalized interchromophore distances obtained by dividing d_{DA} and d_{DD} by the Förster radius for the D–A or D–D pair, respectively; R_0 is Förster radius when κ^2 is $\frac{2}{3}$; n is the refractive index of the solvent and was set to be a constant; N_{A} is Avogadro's number; Q_{D} is the quantum yield of the donor emission; J is the spectral overlap integral between the emission spectrum of the donor and the absorption spectrum of the acceptor. Since FRET is a mechanism for describing energy transfer in the regime of weak electronic coupling, the electronic interactions between all of the chromophores were assumed to be weak and therefore Q_{D} and J were set to be constants. In contrast, d_{DA} , d_{DD} , and κ^2 were adjusted as major variables in the simulations to examine the effect of n_{D} and d_{DD} (and d_{DA}) on η_{FRET} . k_{D} was set to be 1000 ps⁻¹ in the simulations. The orientation factor (κ^2) is defined as follows

$$\kappa^2 = (1 + 3\cos^2\theta) \cos^2\omega$$

where the angle θ represents the angular position of the acceptor relative to the donor's transition dipole vector, and ω is the angle between the acceptor transition dipole vector and the electric field of the donor at the location of the acceptor. Since these angles are assumed to be randomly distributed at the isotropic limit, κ^2 for each FRET pathway can be represented by two random numbers. For cases (i) and (iii) corresponding to the dynamic isotropic limit, κ^2 value was set to be $\frac{2}{3}$, which is the average value of the isotropic distribution. For cases (ii) and (iv) corresponding to the static isotropic limit (Figure S12, Supporting Information), random numbers were generated for the two angles (that is, θ and ω) within the range of 0–2 π , and calculated κ^2 with Equation (4). The approach of calculating η_{FRET} at the dynamic and static isotropic limits used in the simulations is similar to the one used in previous studies on the FRET behavior at those limits.^[21,23]

Frequency-Resolved Femtosecond Transient Absorption Spectroscopy: TA spectra were measured with femtosecond laser pulses using a visible pump–broadband probe scheme. The femtosecond pulses at the center wavelength of 800 nm were generated from a Ti:sapphire amplified laser (Coherent Legend Elite) and split into pump and probe beams. On the pump arm, the 800 nm pulses were converted into the 540 nm pulses with the bandwidth of 16 nm using a home-built, all-reflective-optic non-collinear optical parametric amplifier. Since, at 540 nm wavelength, the absorption of the donor is at least 8 times larger than that of the acceptor, the pump wavelength was selected of 540 nm to preferentially excite donors. The pump pulses were sent through a pair of Brewster-cut fused-silica prisms to precompensate for the dispersion obtained from transmissive optics and compressed to near-transform-limited pulses at the sample position. The pulse energy of the pump pulses was varied from 50

to 200 nj) to check the dependence of transient absorption signal on the excitation energy. It should be noted that, to prevent the excitation of multiple donors, the pump pulses with the pulse energy at the minimal level (50 nj) per pulse) were used for the measurement of TA spectra. On the probe arm, the laser pulses at 800 nm were sent into a sapphire window of 3 mm thickness and converted into white light continuum. The visible portion (460–725 nm) of the white light continuum was used as broadband probe pulses without further compensation of the dispersion. The probe pulses were time-delayed with respect to the pump pulses using a motorized translation stage (Newport, M-ILS150HA). By recording the “pump-on” and “pump-off” probe spectra, the differential transmission ($\Delta T/T$) spectra were obtained as a function of time. The spectra of transient signal and the reference were detected by a spectrometer (Andor, SR303i) equipped with a CCD (Andor, DU420A). In all the TA measurements, the polarization of the pump pulses was set to be at the magic angle (54.7°) relative to the probe polarization in order to prevent the contribution of anisotropic components of the TA signal. For the TA measurement, porphyrin dendrimers were dissolved in tetrahydrofuran (THF). The porphyrin dendrimer solution in THF was prepared with an optical density of ≈ 0.4 at its absorption maximum of 543 nm in THF in a glass cuvette of 1 mm thickness.

Statistical Analysis: Microsoft Excel and OriginPro were used for the statistical analysis of the data presented in this work. The preprocessing and data presentation were performed in the following way. Data in Figure 2c,d represent the averaged η_{FRET} of an individual donor, obtained from 100,000 simulations. The standard error of the mean (SEM) of the η_{FRET} is less than 0.05%. The mean \pm SD of data in Figure 4a are 1.69 ± 0.45 nm. Figure 4b shows mean \pm SD (1.69 ± 0.44 nm). The mean \pm SD of data in Figure 4c are 1.92 ± 0.40 nm (top panel), 2.34 ± 0.61 nm (middle panel), and 2.85 ± 0.76 nm (bottom panel). Table 1 shows mean \pm SD for time constants and β values, which were determined from the global fits of the first and second right singular vectors of TA spectra. Table 1 also shows mean \pm SD of the experimental η_{FRET} . The mean values of theoretical FRET efficiency and modified theoretical η_{FRET} are shown in Table 1, and their SEMs are less than 0.05%.

Supporting Information

Supporting Information is available from the Wiley Online Library or from the author.

Acknowledgements

The authors thank Dae Won Cho and Jaeyoung Sung for their initial help and discussion on the project. This work was supported by the mid-career research project (No. 2020R1A2C3004520) of the National Research Foundation of Korea. This work was supported by the Basic Science Research Program through the National Research Foundation of Korea (NRF) funded by the Ministry of Science, ICT, and Future Planning (No. NRF-2016R1E1A1A01941978). This work was supported by Institute for Basic Science (No. IBS-R004).

Conflict of Interest

The authors declare no conflict of interest.

Keywords

energy transfer, Förster resonance energy transfer (FRET), light harvesting, multichromophore systems

Received: May 2, 2020
Revised: June 24, 2020
Published online: August 19, 2020

- [1] Y. N. Teo, E. T. Kool, *Chem. Rev.* **2012**, *112*, 4221.
- [2] Y. Tachibana, L. Vayssieres, J. R. Durrant, *Nat. Photonics* **2012**, *6*, 511.
- [3] D. Gust, T. A. Moore, A. L. Moore, *Acc. Chem. Res.* **2001**, *34*, 40.
- [4] H. Imahori, *J. Phys. Chem. B* **2004**, *108*, 6130.
- [5] M.-S. Choi, T. Yamazaki, I. Yamazaki, T. Aida, *Angew. Chem., Int. Ed.* **2004**, *43*, 150.
- [6] W.-D. Jang, C.-H. Lee, M.-S. Choi, M. Osada, *J. Porphyrins Phthalocyanines* **2009**, *13*, 787.
- [7] K. Trofymchuk, A. Reisch, P. Didier, F. Fras, P. Gilliot, Y. Mely, A. S. Klymchenko, *Nat. Photonics* **2017**, *11*, 657.
- [8] V. G. Kozlov, V. Bulović, P. E. Burrows, S. R. Forrest, *Nature* **1997**, *389*, 362.
- [9] M. Freitag, J. Teuscher, Y. Saygili, X. Zhang, F. Giordano, P. Liska, J. Hua, S. M. Zakeeruddin, J.-E. Moser, M. Grätzel, A. Hagfeldt, *Nat. Photonics* **2017**, *11*, 372.
- [10] P. K. Santra, P. V. Kamat, *J. Am. Chem. Soc.* **2013**, *135*, 877.
- [11] S. Itzhakov, S. Buhbut, E. Tauber, T. Geiger, A. Zaban, D. Oron, *Adv. Energy Mater.* **2011**, *1*, 626.
- [12] T. Förster, *Ann. Phys.* **1948**, *437*, 55.
- [13] S. A. Latt, H. T. Cheung, E. R. Blout, *J. Am. Chem. Soc.* **1965**, *87*, 995.
- [14] N. Leija-Martínez, S. Casas-Flores, R. D. Cadena-Nava, J. A. Roca, J. A. Mendez-Cabañas, E. Gomez, J. Ruiz-Garcia, *Nucleic Acids Res.* **2014**, *42*, 13963.
- [15] S. Melle, O. G. Calderón, M. Laurenti, D. Mendez-Gonzalez, A. Egatz-Gómez, E. López-Cabarcos, E. Cabrera-Granado, E. Díaz, J. Rubio-Retama, *J. Phys. Chem. C* **2018**, *122*, 18751.
- [16] X. Qiu, J. Guo, Z. Jin, A. Petretto, I. L. Medintz, N. Hildebrandt, *Small* **2017**, *13*, 1700332.
- [17] B. Corry, D. Jayatilaka, P. Rigby, *Biophys. J.* **2005**, *89*, 3822.
- [18] C. Berney, G. Danuser, *Biophys. J.* **2003**, *84*, 3992.
- [19] A. Adronov, S. L. Gilat, J. M. J. Fréchet, K. Ohta, F. V. R. Neuwahl, G. R. Fleming, *J. Am. Chem. Soc.* **2000**, *122*, 1175.
- [20] C. Devadoss, P. Bharathi, J. S. Moore, *J. Am. Chem. Soc.* **1996**, *118*, 9635.
- [21] J. S. Melinger, A. Khachatrian, M. G. Ancona, S. Buckhout-White, E. R. Goldman, C. M. Spillmann, I. L. Medintz, P. D. Cunningham, *ACS Photonics* **2016**, *3*, 659.
- [22] P. K. Dutta, R. Varghese, J. Nangreave, S. Lin, H. Yan, Y. Liu, *J. Am. Chem. Soc.* **2011**, *133*, 11985.
- [23] S. S. Vogel, B. W. van der Meer, P. S. Blank, *Methods* **2014**, *66*, 131.
- [24] N. K. Lee, A. N. Kapanidis, Y. Wang, X. Michalet, J. Mukhopadhyay, R. H. Ebright, S. Weiss, *Biophys. J.* **2005**, *88*, 2939.
- [25] P. Tinnefeld, M. Heilemann, M. Sauer, *ChemPhysChem* **2005**, *6*, 217.
- [26] M. Hoefling, N. Lima, D. Haenni, C. A. M. Seidel, B. Schuler, H. Grubmüller, *PLoS One* **2011**, *6*, e19791.
- [27] E. M. Y. Lee, W. A. Tisdale, A. P. Willard, *J. Phys. Chem. B* **2015**, *119*, 9501.
- [28] S. Buckhout-White, C. M. Spillmann, W. R. Algar, A. Khachatrian, J. S. Melinger, E. R. Goldman, M. G. Ancona, I. L. Medintz, *Nat. Commun.* **2014**, *5*, 5615.
- [29] L. Olejko, I. Bald, *RSC Adv.* **2017**, *7*, 23924.
- [30] L. Gartzia-Rivero, L. Cerdán, J. Bañuelos, E. Enciso, Í. L. Arbeloa, Á. Costela, I. García-Moreno, *J. Phys. Chem. C* **2014**, *118*, 13107.
- [31] C. Vijayakumar, V. K. Praveen, K. K. Kartha, A. Ajayaghosh, *Phys. Chem. Chem. Phys.* **2011**, *13*, 4942.
- [32] W. P. Klein, S. A. Díaz, S. Buckhout-White, J. S. Melinger, P. D. Cunningham, E. R. Goldman, M. G. Ancona, W. Kuang, I. L. Medintz, *Adv. Optical Mater.* **2018**, *6*, 1700679.

- [33] F. Perrin, *Ann. Phys.* **1929**, *10*, 169.
- [34] F. Perrin, *Chem. Rev.* **1930**, *7*, 231.
- [35] C. Y. Wong, C. Curutchet, S. Tretiak, G. D. Scholes, *J. Chem. Phys.* **2009**, *130*, 081104.
- [36] A. Munoz-Losa, C. Curutchet, B. P. Krueger, L. R. Hartsell, B. Men-
nucci, *Biophys. J.* **2009**, *96*, 4779.
- [37] A. I. Fabian, T. Rente, J. Szollosi, L. Matyus, A. Jenei, *ChemPhysChem* **2010**, *11*, 3713.
- [38] Y. Zeng, Y. Y. Li, J. Chen, G. Yang, Y. Li, *Chem. Asian J.* **2010**, *5*, 992.
- [39] R. Berera, R. Van Grondelle, J. T. M. Kennis, *Photosynth. Res.* **2009**, *101*, 105.
- [40] H.-Z. Yu, J. S. Baskin, A. H. Zewail, *J. Phys. Chem. A* **2002**, *106*, 9845.
- [41] A. Lukaszewicz, J. Karolczak, D. Kowalska, A. Maciejewski, M. Ziolk,
R. P. Steer, *Chem. Phys.* **2007**, *331*, 359.
- [42] M. Kullmann, A. Hipke, P. Nuernberger, T. Bruhn, D. C. G. Götz, M.
Sekita, D. M. Guldi, G. Bringmann, T. Brixner, *Phys. Chem. Chem.*
Phys. **2012**, *14*, 8038.
- [43] Y.-H. Jeong, M. Son, H. Yoon, P. Kim, D.-H. Lee, D. Kim, W.-D. Jang,
Angew. Chem., Int. Ed. **2014**, *53*, 6925.
- [44] D. Yim, J. Sung, S. Kim, J. Oh, H. Yoon, Y. M. Sung, D. Kim, W.-D.
Jang, *J. Am. Chem. Soc.* **2017**, *139*, 993.
- [45] I. H. M. van Stokkum, D. S. Larsen, R. van Grondelle, *Biochim. Bio-*
phys. Acta **2004**, *1657*, 82.
- [46] S. S. Vogel, T. A. Nguyen, B. W. van der Meer, P. S. Blank, *PLoS One* **2012**, *7*, e49593.
- [47] J. Szollosi, D. R. Alexander, *Methods Enzymol.* **2003**, *366*, 203.
- [48] T. W. J. Gadella, *FRET and FLIM techniques*, 1st ed.33, Elsevier, Ams-
terdam **2008**.
- [49] H. Langhals, A. J. Esterbauer, A. Walter, E. Riedle, I. Pugliesi, *J. Am.*
Chem. Soc. **2010**, *132*, 16777.
- [50] D. N. H. Meineke, M. L. Bossi, H. Ta, V. N. Belov, S. W. Hell, *Chem.*
– Eur. J. **2017**, *23*, 2469.
- [51] T. Renger, M. Dankl, A. Klinger, T. Schlücker, H. Langhals, F. Müh, *J.*
Phys. Chem. Lett. **2018**, *9*, 5940.
- [52] P. Nalbach, I. Pugliesi, H. Langhals, M. Thorwart, *Phys. Rev. Lett.* **2012**, *108*, 218302.
- [53] H. Langhals, A. Walter, *J. Phys. Chem. A* **2020**, *124*, 1554.
- [54] W. R. Scheldt, J. U. Mondal, C. W. Eigenbrot, A. Adler,
L. J. Radonovich, J. L. Hoard, *Inorg. Chem.* **1986**, *25*,
795.
- [55] W. Yang, B. Li, H. Wang, O. Alduhaish, K. Alfooty, M. A. Zayed, P. Li,
H. D. Arman, B. Chen, *Cryst. Growth Des.* **2015**, *15*, 2000.